Projected Changes in Mean and Extreme Precipitation Over Northern Mexico

Robert H. Nazarian[a] , Noel G. Brizuela[b] , Brody J. Matijevic[a] , James V. Vizzard[a] , Carissa P. Agostino[a] , Nicholas J. Lutsko[b]

[a] *Department of Physics, Fairfield University, Fairfield CT, USA*

[b] *Scripps Institution of Oceanography, University of California at San Diego, La Jolla, CA, USA*

Corresponding author: Robert H. Nazarian, rnazarian@fairfield.edu

ABSTRACT: Northern Mexico is home to more than 32 million people and is of significant agricultural and economic importance for the country. The region includes three distinct hydroclimatic regions, all of which regularly experience severe droughts and flooding and are highly susceptible to future changes in precipitation. To date, little work has been done to characterize future trends in either mean or extreme precipitation over Northern Mexico. To fill this gap, we investigate projected precipitation trends over the region in the NA-CORDEX ensemble of dynamically-downscaled simulations. We first verify that these simulations accurately reproduce observed precipitation over Northern Mexico, as derived from the Multi-Source Weighted-Ensemble Precipitation (MSWEP) product, demonstrating that the NA-CORDEX ensemble is appropriate for studying precipitation trends over the region. By the end of the century, simulations forced with a high emissions scenario project that both mean and extreme precipitation will decrease to the west and increase to the east of the Sierra Madre Highlands, decreasing the zonal gradient in precipitation. We also find that the North American monsoon, which is responsible for a substantial fraction of the precipitation over the region, is likely to start later and last approximately three weeks longer. The frequency of extreme precipitation events is expected to double throughout the region, exacerbating the flood risk for vulnerable communities in Northern Mexico. Collectively, these results suggest that the extreme precipitation-related dangers that the region faces, such as drought and flooding, will increase significantly by the end of the century, with implications for the agricultural sector, economy, and infrastructure.

SIGNIFICANCE STATEMENT: Northern Mexico regularly experiences both severe flooding and droughts, which has significant implications for the region's important agricultural sector. Using high-resolution climate model simulations that have been tested against observations, we find that these hydroclimate extremes are likely to be exacerbated in a warming climate; the drought (flood) season is projected to receive significantly less (more) precipitation (approximately ±10% by the end of the century). Simulations suggest that some of the changes in precipitation over the region can be related to the North American Monsoon, with the Monsoon starting later in the year and lasting several weeks longer. Our results also suggest that the frequency of extreme precipitation will increase, although this increase is smaller than that projected for other regions, with the strongest storms becoming 20% more frequent per degree of warming. These results suggest that this understudied region may experience significant changes to its hydroclimate through the end of the century that will require significant resilience planning.

1. Introduction

Changes in precipitation resulting from anthropogenic global warming are already putting significant stress on human activities, and simulations of future climate scenarios project that the burden of extreme weather and precipitation events is likely to worsen over the coming decades (Donat et al. 2016; Tabari 2020). Adapting to these changes will be a major challenge for a wide variety of stakeholders, and requires detailed and reliable projections of future precipitation. A growing number of studies have sought to provide such projections, primarily focusing on the United States and Europe, where most climate research is carried out (Rajczak et al. 2013; Lopez-Cantu et al. 2020; Nazarian et al. 2022). Unfortunately, this has left large gaps, especially in the Global South, where some of the world's most vulnerable populations reside. Filling out our projections of future changes in precipitation to include regions outside those traditionally studied is an urgent need to ensure equitable access to climate information.

Changes in precipitation patterns resulting from anthropogenic global warming have put additional stress on human activities and increased uncertainty in the management of risk and natural resources. Simulations of future climate scenarios indicate that the burden of extreme weather and precipitation events is likely to worsen over the coming decades (Caparas et al. 2021). Several modeling studies utilizing a high emissions scenario suggest a drier North American Monsoon by the end of the 21st century (Pascale et al. 2017; Colorado-Ruiz et al. 2018; He et al. 2020), thus reducing seasonal precipitation over vast areas of Central and Northwestern Mexico (Almazroui et al. 2021). However, there is uncertainty about the sign of precipitation changes in other regions of Northern Mexico (Caparas et al. 2021; Almazroui et al. 2021), while changes in the seasonality and magnitude of extreme precipitation events have not been systematically studied.

In this study, we take advantage of an ensemble of high resolution climate simulations originally designed to study climate change over the United States, and use it to provide detailed projections of changes in mean and extreme precipitation over Northern Mexico (see territorial definition in Fig. 1), which is home to 32 million people and includes numerous areas with high risk and and vulnerability to drought, heatwaves, and flooding (Ortega-Gaucin and Velasco 2013; Díaz Caravantes et al. 2014; Aguilar-Barajas et al. 2019). The region accounts for 27% of Mexico's gross area dedicated to agriculture and 32% of its agricultural revenue (INEGI 2020), and without proper adaptation, substantial precipitation changes as a result of future warming could lead to major social and economic disruptions (Magaña et al. 2021). Policies for climate adaptation in this region must account for possible changes in mean and extreme precipitation patterns over the coming decades, but studies of projected precipitation changes in Northern Mexico are currently lacking.

To study future trends in mean and extreme precipitation over the region, we use the COordinated Regional climate Downscaling EXperiment (CORDEX) ensemble, which consists of dynamically-downscaled Global Climate Model (GCM) simulations, derived from the Fifth Climate Model Intercomparison Project (CMIP) ensemble. Several studies have shown that dynamically-downscaling GCM simulations using high resolution Regional

Climate Models (RCMs) can provide "added value" by capturing smaller-scaled climate processes compared to using GCMs (Diffenbaugh et al. 2005; Di Luca et al. 2012; Ashfaq et al. 2016; Lucas-Picher et al. 2017). Of particular relevance here, RCMs better capture the mesoscale phenomena, such as mesoscale convective systems (MCS), that lead to extreme precipitation. In addition to this improvement, RCMs also afford more realistic representations of surface forcing, such as orography, (Leung et al. 2003) and of the atmosphere's regional-scale circulation, both of which contribute to more realistic projections of extreme precipitation, though neither GCMs nor RCMs are able to accurately simulate extreme precipitation due to convection (O'Gorman 2015; Muller and Takayabu 2020).

We focus specifically on the NA-CORDEX ensemble, which provides downscaled simulations over the North American region (with approximate longitudinal bounds of 62°W to 169°W and latitudinal bounds of 19°N to 68°N), including Northern Mexico. NA-CORDEX has been used to investigate future climate change over the United States (Bukovsky and Mearns 2020; Lopez-Cantu et al. 2020; Nazarian et al. 2022), but to our knowledge has not previously been used to study climate change over Mexico specifically. The NA-CORDEX domain does not extend over the entire country of Mexico, but does include a significant portion of the country, including the entirety of Northern Mexico, which has three broad precipitation regimes: Northwestern Mexico, which receives rainfall in Winter from atmospheric rivers (Rutz and Steenburgh 2012); Baja California Sur and the Northern Mexican highlands, which are characterized by dry and hot Springs, followed by heavy precipitation from mid- to late-Summer when the North American Monsoon is active (Adams and Comrie 1997); and Northeastern Mexico (Nuevo León, Tamaulipas), where Fall precipitation is largely driven by tropical cyclones (Breña Naranjo et al. 2015) and intra-seasonal southward moisture transport from the North American Great Plains (Mo 2000; Jáuregui 2003).

We begin by assessing the ability of the NA-CORDEX to simulate present-day precipitation over Northern Mexico by comparing historical simulations with observations derived from the Multi-Source Weighted-Ensemble Precipitation (MSWEP) product in Section 3. After demonstrating that NA-CORDEX accurately reproduces observed rainfall statistics,

we quantify future trends in mean and extreme precipitation over the region in Sections 4a and 4b, respectively. Given the role of the North American monsoon on the seasonality of extreme precipitation over Northern Mexico, we investigate changes in the characteristics of the monsoon in Section 4c, including its onset timing and length. In Section 4d, we focus in on five cities, representing different regions of Northern Mexico, as case studies for future trends in extreme precipitation. We provide a synthesis of results and discuss implications in Section 5.

2. Methods

a. The NA-CORDEX ensemble

To diagnose future changes in precipitation over Northern Mexico, we use the dynamically-downscaled NA-CORDEX ensemble. CORDEX downscales a suite of GCMs from CMIP5 using a number of RCMs (see Table 1 for a list of the GCM and RCM pairings). CORDEX is ideal for studying regional changes in hydroclimate and has been employed in numerous studies of other regions (Lopez-Cantu et al. 2020; Rendfrey et al. 2021; Nazarian et al. 2022).

We use the NA-CORDEX simulations run at 0.22° (~25 km) horizontal resolution, as previous studies have shown that higher resolution models provide more accurate estimates of precipitation (Lucas-Picher et al. 2017). The only set of NA-CORDEX simulations conducted at higher resolution were forced with reanalysis data, and so cannot be used to make climate projections. 0.22° resolution is sufficiently high to capture hydroclimate variations over Northern Mexico, which we define to include the states of Baja California, Baja California Sur, Sonora, Chihuahua, Durango, Sinaloa, Nuevo León, Tamaulipas, and Coahuila (see Fig. 1 for an illustration of this region). All variables are taken at the surface; data at higher atmospheric levels are not publicly available. We use data that have been bias-corrected using the daily Daymet observational dataset, which is accepted practice

for studying climate impacts (Kirchmeier-Young et al. 2017; Cannon 2018; McGinnis and Mearns 2021; Nazarian et al. 2022).

Global Model	Regional Model	ECS (°C)
CanESM2	CanRCM4	3.7
	CRCM5-UQAM	3.7
GEMatm-Can	CRCM5-UQAM	3.7
GEMatm-MPI	CRCM5-UQAM	3.6
GFDL-ESM2M	RegCM4	2.4
	WRF	2.4
HadGEM2-ES	RegCM4	4.6
	WRF	4.6
MPI-ESM-LR	CRCM5-UQAM	3.6
	RegCM4	3.6
	WRF	3.6
MPI-ESM-MR	CRCM5-UQAM	3.4

Table 1. Global and regional model pairings of the 12 available NA-CORDEX simulations with daily, bias-corrected output at 0.22° (~25 km) resolution and forced using the RCP 8.5 scenario. The equilibrium climate sensitivity (ECS; the temperature change due to a doubling of CO_2), as diagnosed by the NA-CORDEX team (see https://na-cordex.org/simulation-matrix.html), is noted for each model.

While the NA-CORDEX simulations span 1950-2100, we focus on two twenty-year periods. We take the "historical" period to be 1986-2005, the "projected" period to be 2081-2100, and report changes as the difference between the two (i.e. projected minus historical). Unless otherwise stated, we use daily-averaged values for all variables. The simulations are forced with the RCP8.5 emission scenario (i.e., a "high emissions" scenario) for the period 2006-2100. While it is too soon to know which emissions pathway we will follow through the end of the century, we utilize RCP8.5 since there are more NA-CORDEX simulations conducted using this emissions scenario than there are for the other emissions scenarios. Fractional changes in extreme precipitation are independent of the emissions scenario (Pendergrass et al. 2015), so we do not expect this choice to have a significant impact on our results. In total, data from 12 simulations are available (Table 1), but we

exclude one model pairing (CanESM2, CRCM2-UQAM) which produces an exceptionally large drying over the entire region. Investigating why this pairing produces such outlier behavior is a topic of future work.

Even with one simulation excluded, the range of equilibrium climate sensitivities across the simulations is 2.4-4.6°C [for reference, the range of equilibrium climate sensitivity of the full CMIP5 ensemble ranges is 2.0-4.7°C (Andrews et al. 2012; Flato et al. 2014)]. Furthermore, the spread in annual-mean North American precipitation projections from the downscaled NA-CORDEX simulations is greater than that of the driving GCMs alone, and closer to that of the full CMIP5 ensemble (Bukovsky and Mearns 2020). Regardless of the global or regional model used, all simulations slightly underestimate the magnitude of average annual, accumulated precipitation over the region (approximately 0.473 m, based on data from the MSWEP [see next section]).

b. MSWEP

MSWEP (version 2.8) is a global precipitation product that uses a combination of gauge-, satellite-, and reanalysis-based data (Beck et al. 2017, 2019). The MSWEP dataset begins in 1979 and continues through the present. MSWEP is ideal for studying regional hydroclimate given both its high spatial (0.1°) and temporal (3 hour) resolution and, as such, has been used in a number of earlier studies (Sharifi et al. 2019; Xu et al. 2019; Li et al. 2022). Furthermore, it is the only product to use a combination of gauges, satellites, and reanalyses to derive precipitation observations, which has been shown to particularly enhance its performance over convective- and frontal-dominated weather regimes (Beck et al. 2017). Furthermore, the MSWEP data uses an algorithm to account for gauge reporting times, which minimizes the mismatch between gauge observations and satellite/reanalysis estimates. We refer the reader to Beck et al. (2019) for more information about the data.

Like the NA-CORDEX historical output, we take the MSWEP data from 1986 to 2005. MSWEP and NA-CORDEX have different resolutions (0.10° vs. 0.22°, respectively), so we re-grid both datasets to a common grid to perform the comparison. We evaluate the

skill of the NA-CORDEX ensemble by calculating the correlation coefficients between the NA-CORDEX ensemble average and the average of MSWEP observations. We do not detrend the MSWEP observations nor NA-CORDEX simulations to perform this comparison since we are conducting this comparison over the historical period.

c. North American Monsoon

The North American Monsoon (hereafter NAM) is responsible for providing approximately 70% of the annual precipitation over the western portion of Northern Mexico (Reyes et al. 1994). While the dynamics governing the NAM are unique from other monsoons (notably the Indian monsoon), it is nevertheless characterized as a monsoon by its confinement to the Summer months and its reversal of the surface winds (Barlow et al. 1998; Boos and Pascale 2021).

To study the projected changes in the NAM we define the NAM region to include the states of Baja California Sur, Sonora, Sinaloa, Chihuahua, and Durango, though we note that the precipitation each of these states experiences due to the monsoon may vary significantly. In order to calculate the timing of the NAM, we utilize the metric of Zhang et al. (2002), which defines the start of the monsoon as the first day on which a five-day running mean rainfall index exceeds 2 mm (this value is modified from the original Zhang et al. (2002) metric given the amplitude of the NAM relative to other monsoons) and persists continuously for five days. The monsoon state is the period over which at least 10 out of every 20 days receive more than 2 mm of precipitation, with the end of the monsoon defined as when this criterion is no longer satisfied. We note that this metric is similar to that of Geil and Serra (2013), although we use a slightly larger threshold value (2 mm compared to their 1.3 mm) due to the NA-CORDEX climatology. For each simulation, as well as for the MSWEP record, the monsoon start and end dates are calculated each year before any averaging is conducted.

d. Extreme Precipitation Metrics

Numerous metrics for extreme precipitation have been defined in the literature, such as the annual maximum of daily precipitation [Rx1day], the number of a days in a year with precipitation exceeding 10mm [R10mm], and the 99th percentile of precipitation [R99] (Schär et al. 2016; Nazarian et al. 2022). Unless otherwise noted, we use the R99 metric in our analysis, as it is the most commonly used metric in the regional climate change literature (Schär et al. 2016) and is of most use to planners and water managers. All days are used to calculate extreme precipitation statistics (Ban et al. 2015; O'Gorman 2015), rather than wet days only, since the frequency of wet day does not necessarily remain fixed in a warming climate (Schär et al. 2016).

Furthermore, we perform a similar frequency analysis as in Martinez-Villalobos and Neelin (2019) by considering daily, regionally-averaged (weighted by area) mean and extreme precipitation for each simulation. Values are then averaged across the 11 simulations to derive the ensemble average. Finally, we calculate fractional changes in extreme precipitation (i.e. the percent change in R99 per degree warming), using local, rather than global, warming. Although previous studies have calculated this ratio using global-mean warming, we instead use local warming so as to provide regional stakeholders with a more localized planning metric. We also believe that the local change in temperature is more informative for diagnosing the drivers of precipitation changes at the regional scales considered here, despite being more uncertain than the global increase in temperature.

3. Model Assessment

There are two prominent wet areas in Northern Mexico: one on the windward side of the Sierra Madre Mountain Range that is influenced by the NAM (Adams and Comrie 1997; He et al. 2020) and another along the Gulf of Mexico for which late Summer precipitation is governed by tropical cyclones and intraseasonal moisture fluxes from the North American Great Plains (Mo 2000; Jáuregui 2003) (Figure 1b). Between these regions, central Northern

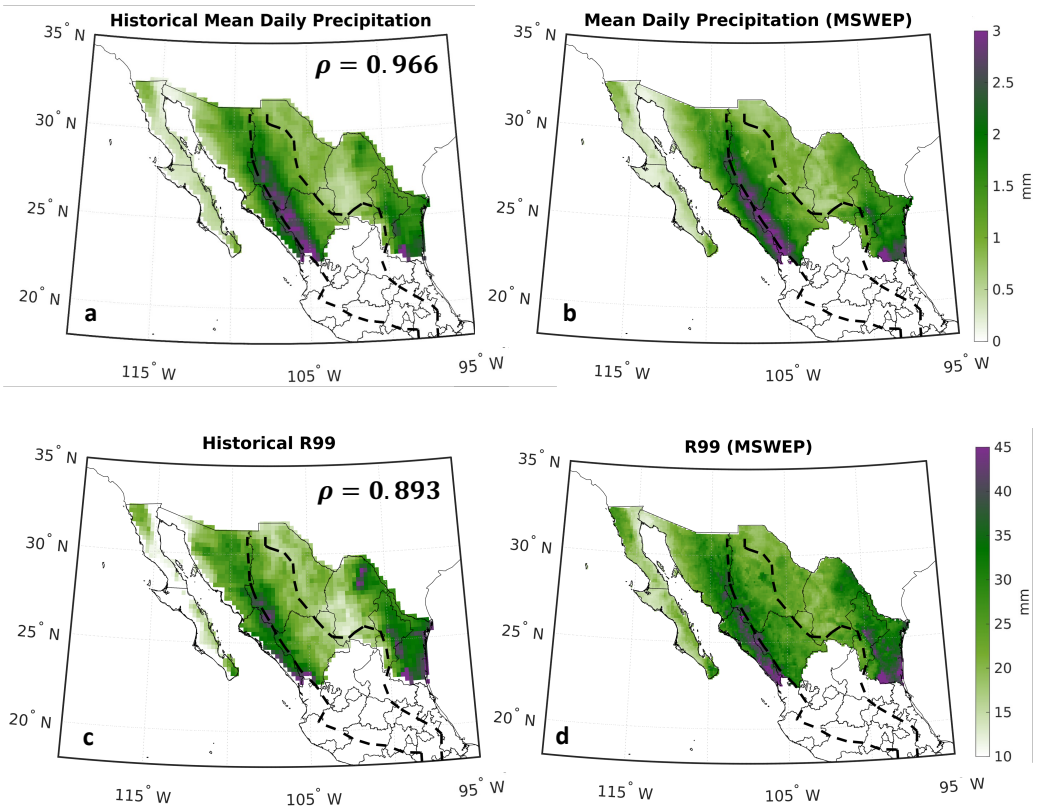

Figure 1. Comparison between (a,b) mean and (c,d) R99 daily precipitation in historical (a,c) NA-CORDEX simulations and (b,d) MSWEP data. The correlation coefficients ρ quantify the agreement between model output and observations. The black dashed line denotes the Sierra Madre Mountain Range.

Mexico is drier, while the Baja California peninsula in the far west, which relies heavily precipitation from tropical cyclones (Breña Naranjo et al. 2015), is extremely dry (generally less than 0.5mm/day).

In the ensemble-mean, the historical NA-CORDEX simulations accurately capture the spatial distributions of annual-mean and R99 daily precipitation when compared to MSWEP observations (Figure 1), with correlation coefficients (ρ) between observed and simulated mean and R99 of $\rho = 0.966$ and $\rho = 0.893$, respectively. Similar skill is seen for individual

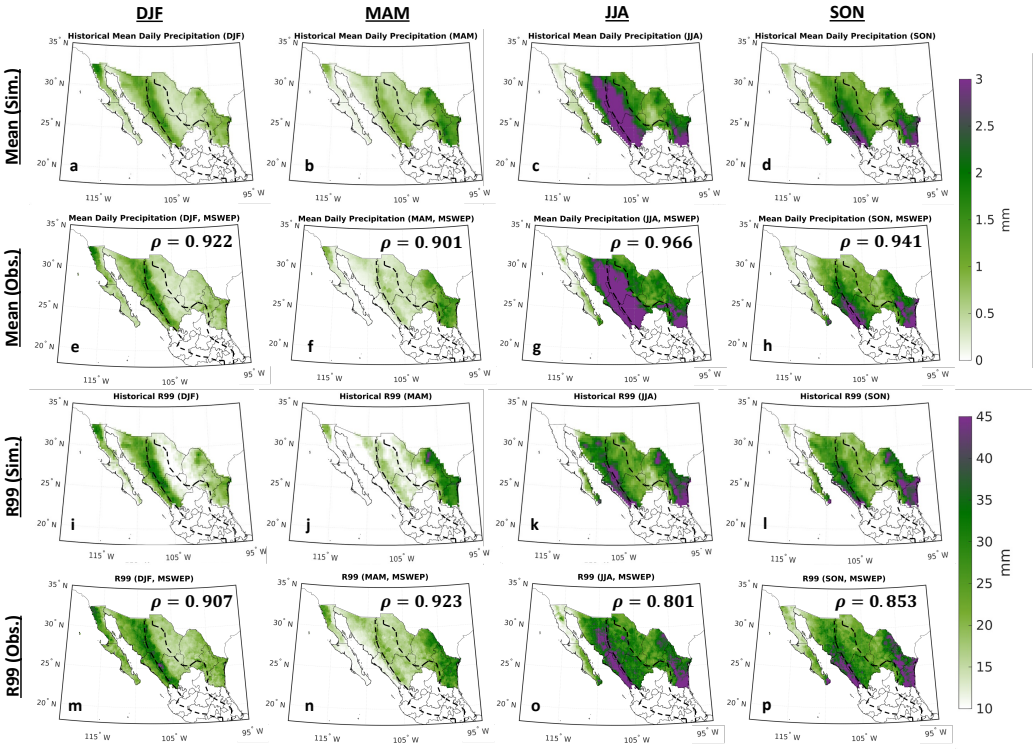

Figure 2. Comparison between seasonal (top two rows) mean and (bottom two rows) R99 daily precipitation in historical NA-CORDEX simulations and MSWEP data. The correlation coefficients (ρ) in the second and fourth rows quantify the agreement between model output and observations. As in Figure 1, the black dashed line denotes the Sierra Madre Mountain Range.

seasons in Fig. 2, though model skill in R99 tends to be slightly higher in Winter and Spring (December-January-February, DJF; March-April-May, MAM) and lower in Summer and Fall (June-July-August, JJA; September-October-November, SON) while the converse is true for model skill in mean precipitation.

Inspection of historical model output and MSWEP data (Figure 1a,b) suggests that simulated mean precipitation rates are very close to observed rates, with a small dry bias in Coahuila and Tamaulipa. Biases in extreme precipitation differ slightly, featuring an un-

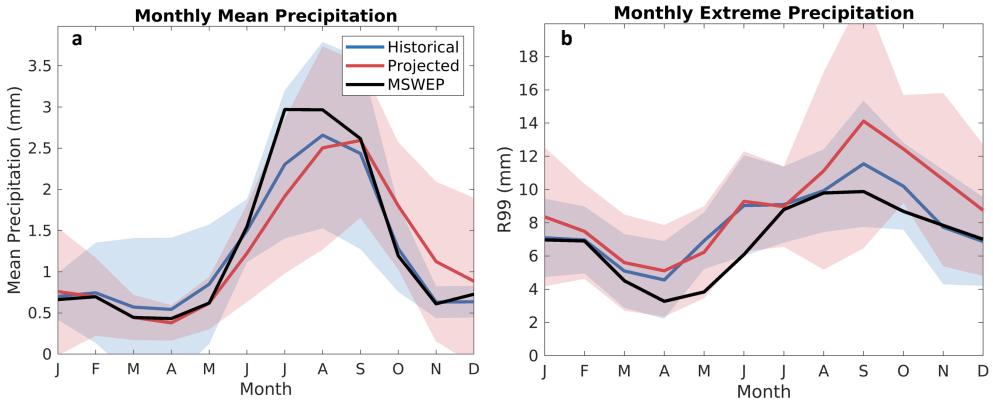

Figure 3. Seasonal evolution of (a) mean daily and (b) R99 precipitation over all of Northern Mexico in (black) MSWEP data, (blue) historical, and (red) end-of-century simulations. Solid lines indicate the multi-model means, while shading represent the 90% confidence intervals.

derestimation of R99 throughout most of the region. The dry bias is most pronounced in the California Peninsula and in the central NAM region (Figure 1c,d). These deficiencies are generally most notable in Summer and the best agreement is seen in the Winter/Spring (Figure 2).

Monthly averages of mean and R99 precipitation over all of Northern Mexico (Figure 3) help further diagnose biases in modelled precipitation. The biases in model-based estimates of the mean daily precipitation are greatest during the beginning of the wet season, during which the model underestimates the magnitude of daily precipitation (note, however, that Figure 2 illustrates that models capture the spatial pattern of summertime precipitation well). Model estimates of the monthly R99 over Northern Mexico are biased high for all seasons except Winter (Figure 3b). Despite these differences, MSWEP-based estimates of mean and extreme precipitation always fall within the 90% confidence intervals (calculated from the inter-model spread) of the historical simulations from the NA-CORDEX ensemble (Figure 3a,b), except for the month of May for R99. Taken together, Figures 1 through 3 demonstrate that the NA-CORDEX simulations accurately capture both the spatial distributions and the seasonalities of historical mean and extreme precipitation over Northern Mexico, suggesting

that the NA-CORDEX ensemble is a viable tool for studying projected future changes over the region.

4. Projected Changes in Mean and Extreme Precipitation

a. Changes in mean precipitation

In the ensemble-mean, the NA-CORDEX ensemble projects a decrease in precipitation where it is presently high and an increase in precipitation where it is presently low (Figures 4a and 2a-d). Decreases of up to -0.2mm/day ($\approx -7\%$) are seen along the western slopes of the Sierra Madre and along the Huasteca region in Southern Tamaulipas, and increases of up to +0.2mm/day are projected for most of Sonora, Coahuila, Baja California, and Nuevo León (Fig. 4a). This is in contrast to temperature, which increases more uniformly over the region (not shown).

Individual simulations in the NA-CORDEX ensemble project changes in mean precipitation of similar magnitudes, but exhibit some diversity in the spatial patterns of change (Figure 5). Such variation among simulations is largely due to the regional models, as ensemble members with the same driving model exhibit different spatial patterns of change – compare, for example, the simulations using the MPI-ESM-LR global model in Figure 5h-j.

Examining the changes in the seasonal cycle of precipitation over Northern Mexico (Figures 3a and 4b-e) shows a delay in the arrival of the wet season under the high emissions scenario. This change results in a drier Spring (MAM, Figure 4b) and Summer (JJA, Figure 4c) with a wetter Fall (SON, Figure 4d), putting additional stress on water resources during some of the warmest months of the year. The reduced mean precipitation along the western edge of the Sierra Madre highlands is consistent with drying of the NAM, which previous studies have discussed (Almazroui et al. 2021; He et al. 2020). We explore the change in NAM characteristics further in Section 4c.

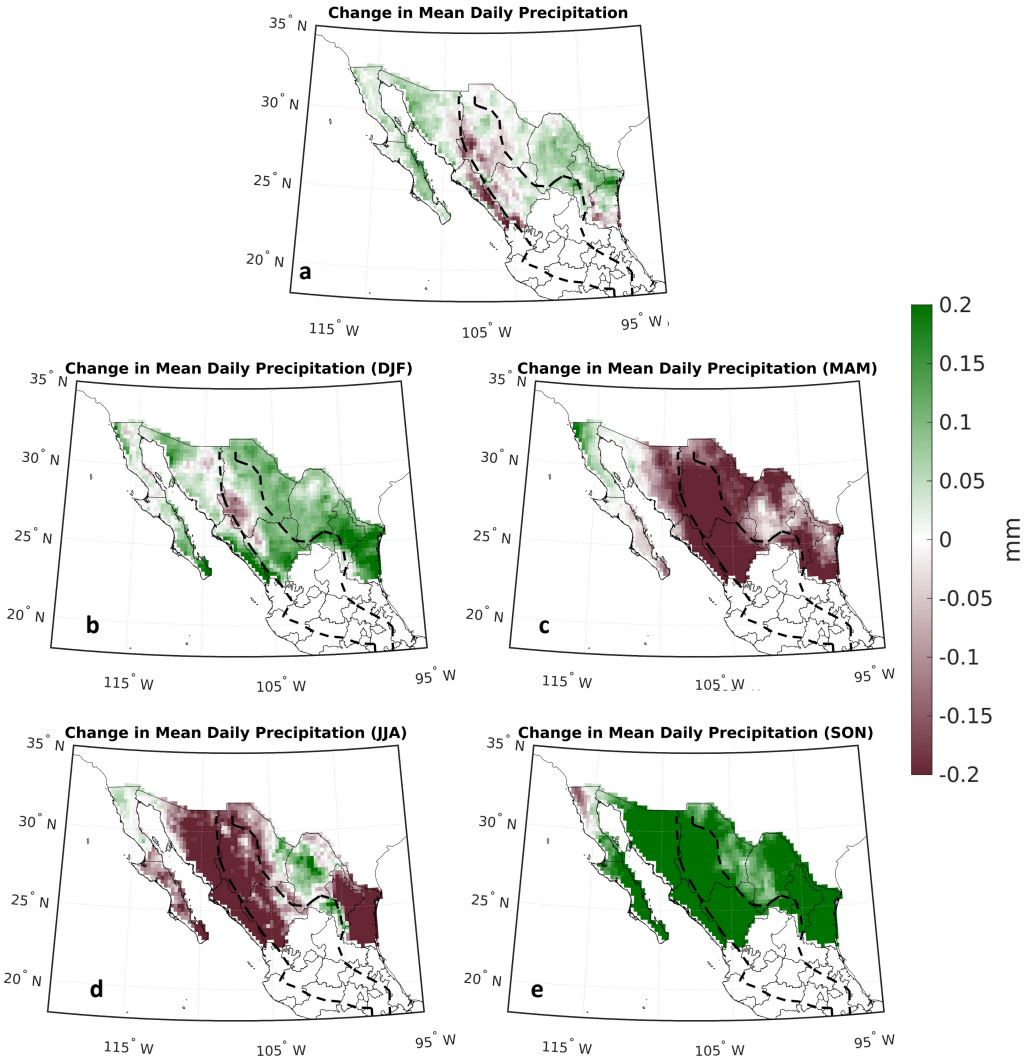

278 Figure 4. Ensemble average change (projected minus historical) in (a) annual and (b-e) seasonal mean
279 precipitation from NA-CORDEX. The dashed contour delineates the Sierra Madre highlands.

303 Projected precipitation changes outside the NAM region follow a variety of patterns
304 in seasonality and magnitude (Figure 4). There is substantial intermodel spread in the
305 projections for the northwestern and northeastern corners of the country (Figure 5), but a
306 seasonal breakdown provides greater clarity. In Baja California, precipitation is projected to

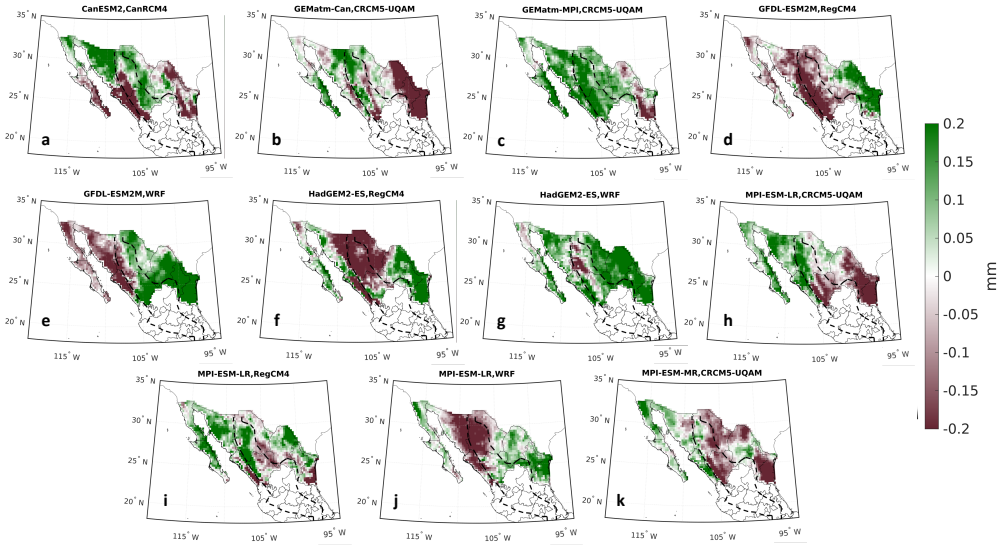

Figure 5. Change in mean precipitation from NA-CORDEX for the 11 ensemble members considered in this analysis. Dashed line delineates the Sierra Madre highlands.

decrease during Fall but increase throughout the rest of the year (Figure 4), possibly pointing to changes in the timing and intensity of the atmospheric rivers that drive the wet season between November and April in this area (Dettinger et al. 2011). In the northeast corner of our study region (Tamaulipas and Nuevo León), precipitation is projected to increase during Fall and Winter but decrease during Spring and Summer (Figure 4). Taken together, this suggests that some of the simulations struggle to capture changes in atmospheric rivers over the region. For instance, simulations using GFDL's ESM2M project a significantly weakened atmospheric river. Therefore, while the NA-CORDEX ensemble reasonable captures the historical precipitation over the region, all ensemble members may not capture the physics responsible for changes in atmospheric rivers and the associated precipitation in a warming climate. We discuss regional variations in projected seasonality of precipitation changes in more detail in Section 4d.

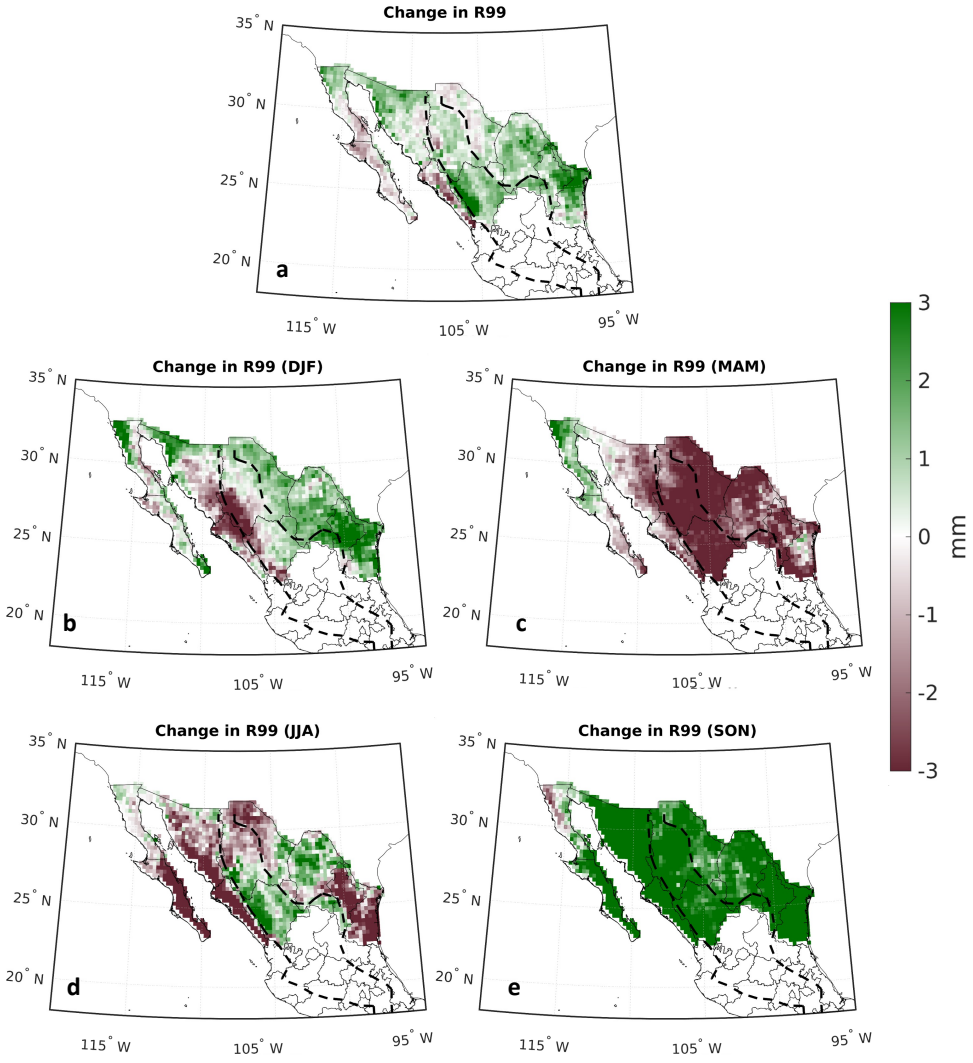

Figure 6. As in Figure 4, but now for extreme precipitation (R99).

b. Changes in extreme precipitation

Extreme precipitation events are projected to intensify during the wet season and weaken during the dry season (Figure 6): throughout most of Northern Mexico, the magnitude of R99 precipitation events increases by > 3 mm day^{-1} during the wet season (Figure 6e) and decreases by a similar amount during the dry season (Figure 6c). These changes resemble

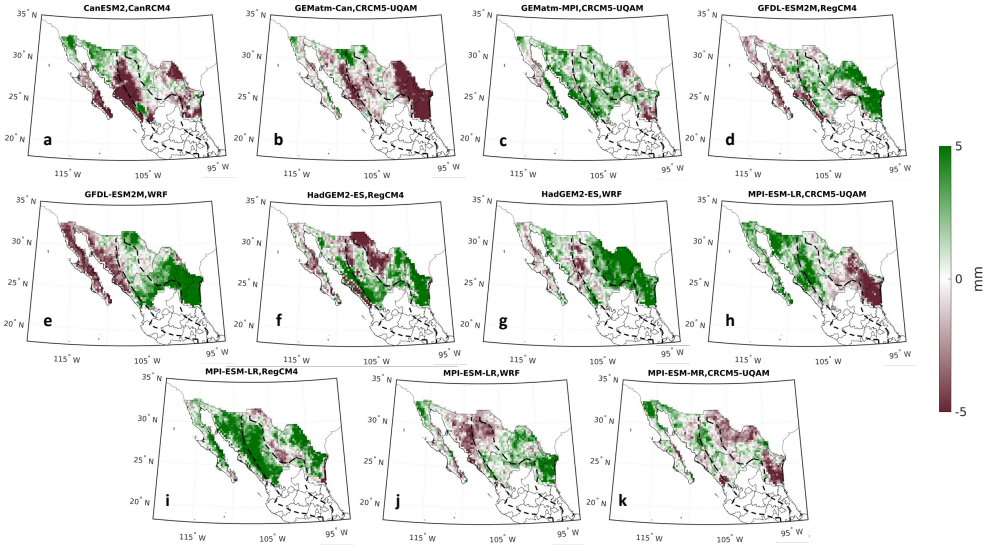

Figure 7. As in Figure 5, but now for extreme precipitation (R99).

the seasonal and spatial patterns in projections of mean precipitation (Figure 4) and could bring about increased risk of flood and water shortages during the wet and dry seasons, respectively.

Projected changes in precipitation extremes show substantial variations across the 11 models considered here (Figure 7), but agreement across models is better when broken down by season (Figure 8). Intermodel spread is largest in Winter (Figure 8b) and Summer (Figure 8d), and there is closer agreement for projections of a drier dry season (MAM, Figure 8c) and a wetter wet season (SON, Figure 8c). The increased magnitude of R99 during the Fall suggests increases in the frequency and/or severity of tropical cyclones originating in the Eastern Pacific and North Atlantic basins, and we discuss this in more detail in Section 5. Likewise, potential changes in the seasonality of the NAM, such as a later onset and longer duration, could explain the large increase in Fall extreme precipitation, and we return to this in Section 4c.

We also consider changes in the frequencies of the strongest storms in Figure 9. Projections suggest that moderate storms (i.e. 90th percentile events) will increase in frequency by

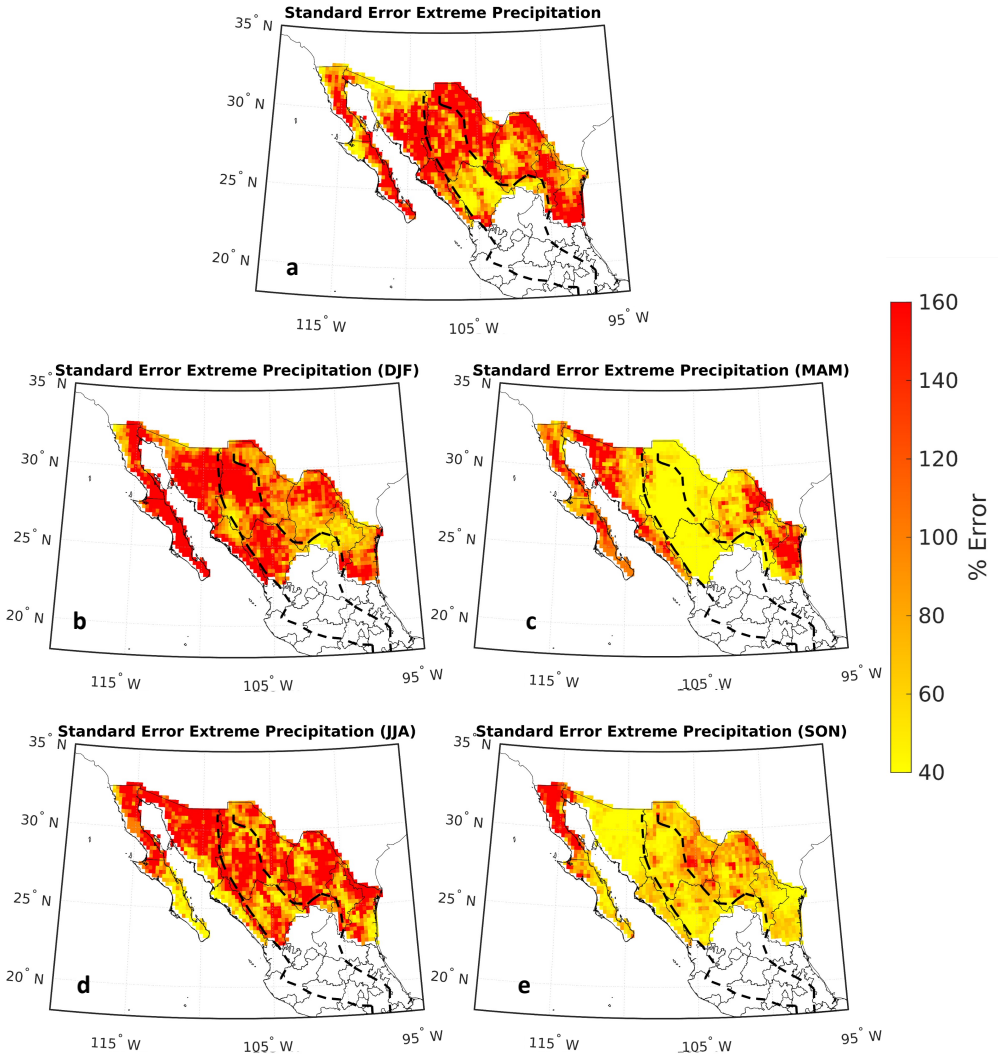

Figure 8. As in Figure 6, but now for multi-model standard error in the change in extreme precipitation.

approximately 10% per degree of local warming, while the strongest storms (i.e. the 99.99th percentile) will increase in frequency by approximately 20% per degree of local warming. Since the region is projected to warm by approximately 4°C in the multi-model mean, this implies a near-doubling of the frequency of the strongest storms. While large, we note that this increase is much smaller than that of other regions, such as the Northeast

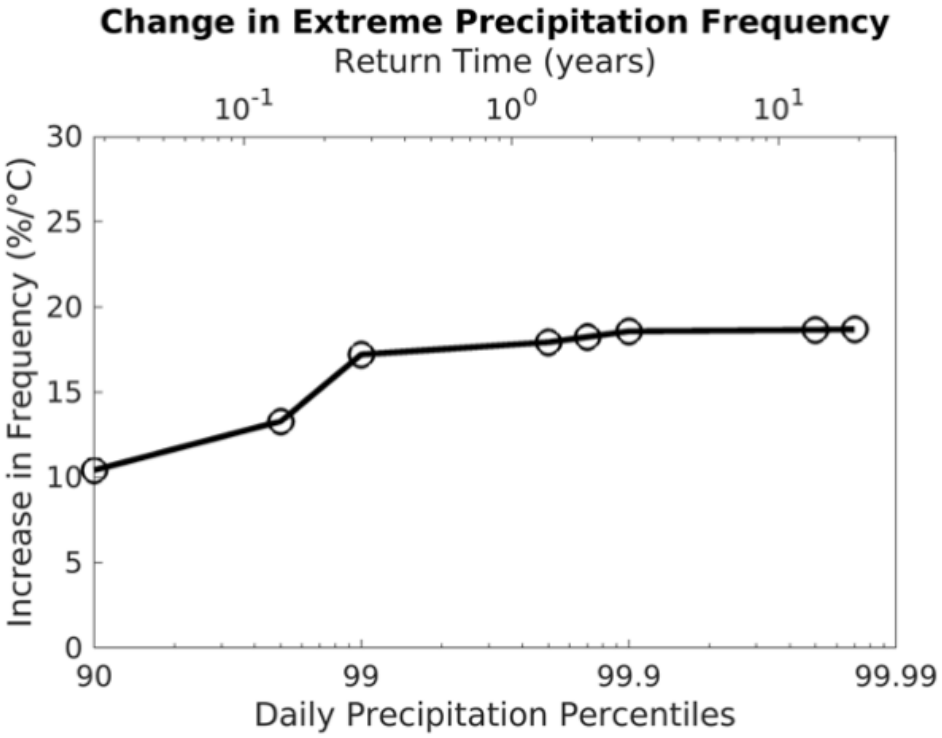

337 Figure 9. Ensemble-averaged change in storm frequency (as measured through various percentiles)
338 per degree of local warming. Corresponding return times are noted; for example the change in the
339 frequency of the (historical) 99.9 percentile storm is equivalent to the change in frequency of the ~1-in-3
340 year storm. While not shown here, there is larger intermodel spread for higher percentiles, given the
341 increasingly small sample size.

349 US (Nazarian et al. 2022) and Central Europe (Myhre et al. 2019), which are projected to
350 experience a doubling in frequency per degree of local warming (i.e., 100%/°C) for the
351 strongest storms.

354 To diagnose the potential drivers of the changes in extreme precipitation over the region,
355 we calculate the fractional changes (Figure 10). Extreme precipitation is generated by

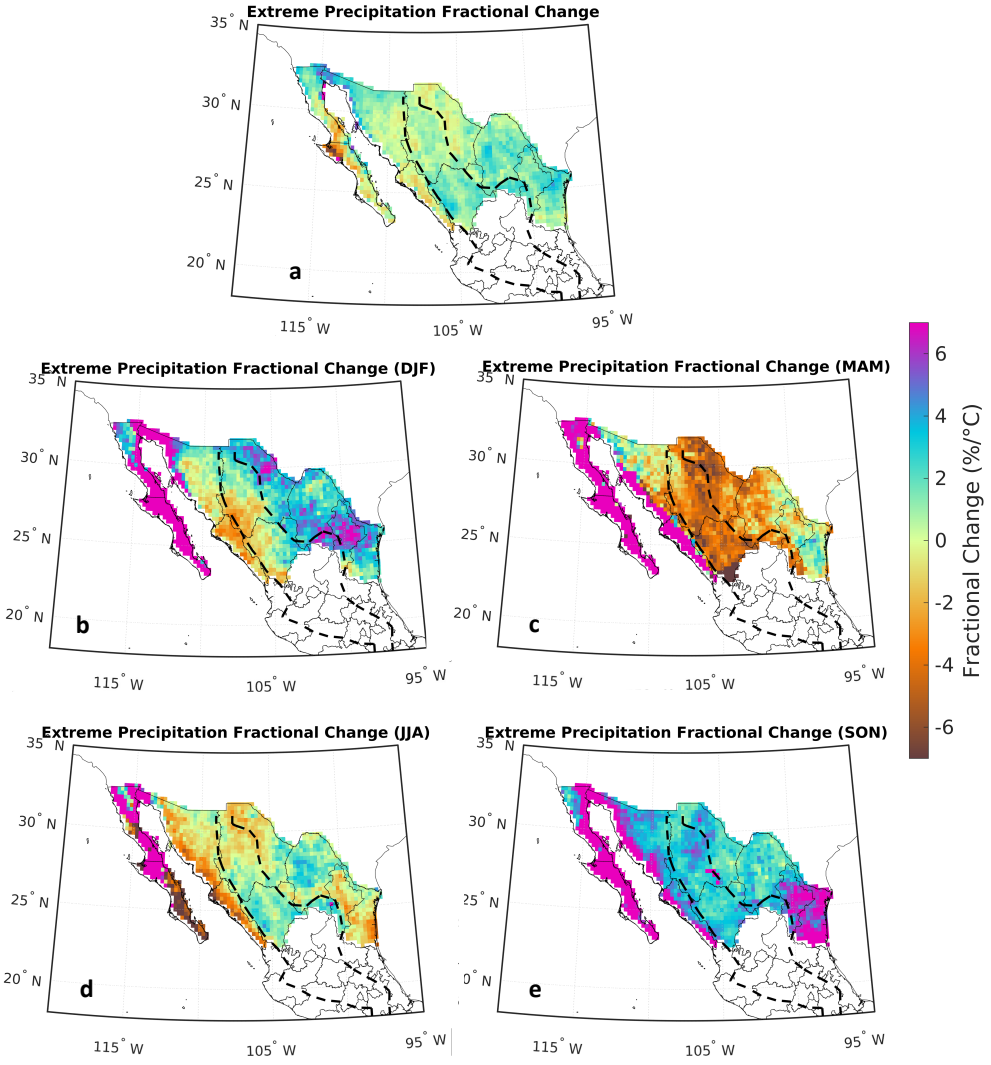

Figure 10. As in Figure 6, but now for the fractional change in extreme precipitation.

strong updrafts, such that the rate of extreme precipitation (P_e) can be approximated as:

$$P_e \approx \int -\rho w \left(\frac{dq_s}{dz}\right) dz, \tag{1}$$

where ρ is the air density, w is the vertical velocity, q_s is the saturation specific humidity, and z is the vertical coordinate. This expression can be used to decompose fractional changes

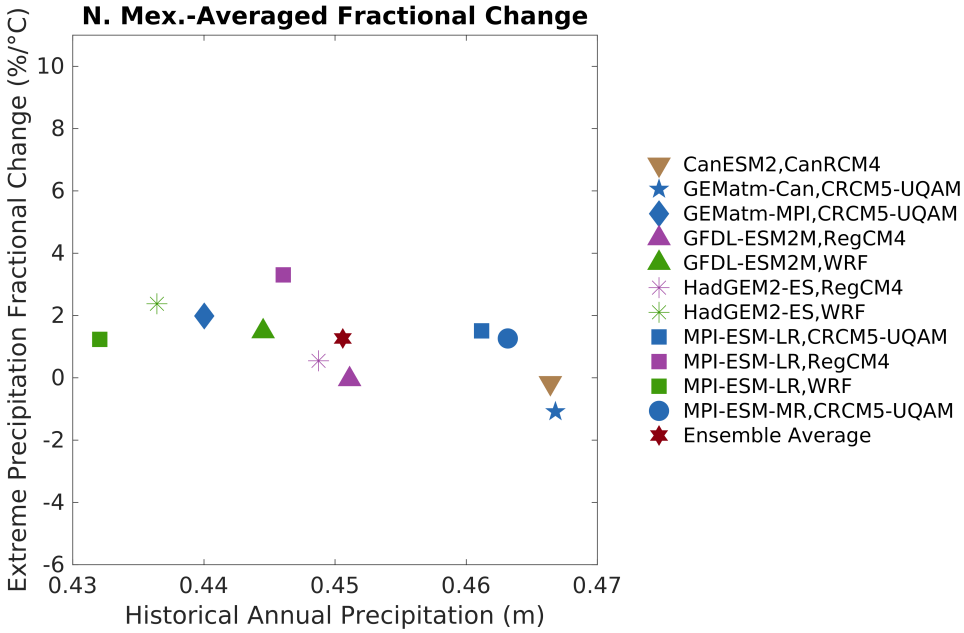

Figure 11. Fractional changes in ensemble-average extreme precipitation. Each GCM has a unique marker and each RCM has a unique color.

in P_e as:

$$\frac{\delta P_e}{P_e} = \underbrace{\left(\frac{\int \rho w\, \delta(\frac{dq_s}{dz})dz}{\int \rho w(\frac{dq_s}{dz})dz}\right)}_{\text{thermodynamic}} + \underbrace{\left(\frac{\int \delta(\rho w)(\frac{dq_s}{dz})dz}{\int \rho w(\frac{dq_s}{dz})dz}\right)}_{\text{dynamic}} + \underbrace{\left(\frac{\int \delta\left(\rho w(\frac{dq_s}{dz})\right)dz}{\int \rho w(\frac{dq_s}{dz})dz}\right)}_{\text{nonlinear}} \tag{2}$$

where δ is the difference between the projected and historical periods. The first term is the thermodynamic contribution to the change in extreme precipitation which, from the Clausius-Clapeyron relation, is approximately +6-7%/°C. The second term is the contribution from dynamical changes, and is typically ± 2%/°C (O'Gorman 2015). The final term

combines nonlinear changes, changes in precipitation efficiency (Lutsko and Cronin 2018; Abbott et al. 2020) and any sources of error, which are typically small.

As mentioned in Section 2, all fractional changes are taken with respect to local, rather than global, temperature changes. We cannot explicitly calculate the individual terms in (2) since only surface-level data is publicly-available and individual modeling centers were only able to provide data at a few vertical levels, which are insufficient to calculate vertical integrals. We therefore compare the fractional increases in extreme precipitation with the thermodynamic rate of ~6-7%/°C and interpret departures from this rate as likely reflecting dynamical changes. We caution however, that departures from Clausius-Clapeyron scaling might also be due to microphysical responses or nonlinear effects[1].

The fractional change in annual extreme precipitation is small and positive over most of the region, with an average of approximately 2%/°C (Figure 10). This suggests a strong dynamical damping of changes in extreme precipitation over the region. The fractional changes are generally highest in Fall (Figure 10e), but are still below 7%/°C over the majority of the region. In Spring (MAM) fractional decreases of up to -3%/°C are seen in much of the region. These seasonal changes in the fractional change partly reflect changes in the timing of extreme precipitation due to the monsoon.

c. Changes in NAM characteristics

The changes in the seasonality of mean and extreme precipitation seen in Figures 4 and 6 are likely due at least in part to the changing NAM. To investigate this link, we start by considering the seasonality of precipitation over the states that experience the NAM: Baja California Sur, Sonora, Chihuahua, Sinaloa, and Durango. Like Figure 3, Figure 12 shows a several week delay in the timing of the high precipitation season. The shift in the seasonality of both mean and extreme precipitation over the region also exhibits a longer tail in the Fall-time, with the end period of the monsoon becoming more protracted and less sudden (not shown).

[1]Though consistency across models suggests changes are likely driven by dynamics rather than microphysics.

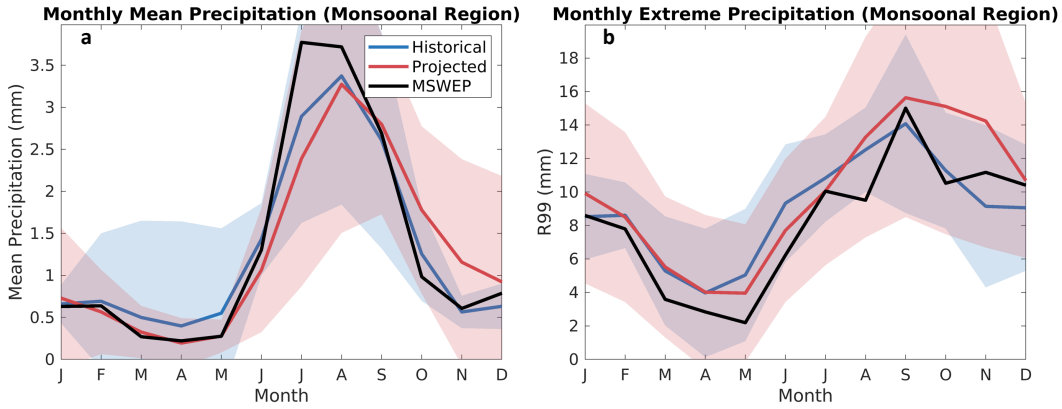

Figure 12. As in Figure 3, but now considering just the states that experience that NAM.

	MSWEP	Ens. Av. (H)	St. Err. (H)	Ens. Av. (P)	St. Err. (P)	Change
Start	June 26	June 5	16 days	June 12	18 days	+7 days
End	Sep. 24	Sep. 16	13 days	Oct. 7	10 days	+21 days
Length	90 days	103 days	16 days	117 days	22 days	+14 days

Table 2. Comparison of North American Monsoon statistics in MSWEP and NA-CORDEX simulations, as calculated with the modified Zhang et al. (2002) metric. Statistics for historical and projected periods are denoted by H and P, respectively. The final column indicates the change in the ensemble average (projected minus historical), and indicates that the NAM is expected to start and end later, and last longer.

The North American Monsoon is not the only physical process that contributes to precipitation over this sub-region, so we use the Zhang et al. (2002) metric described in Section 2 to specifically diagnose changes in the monsoon timing and length. Results are presented in Table 2. Before considering projected changes in the NAM using NA-CORDEX, we compare the simulated historical NAM with observations. NA-CORDEX exhibits an early bias to the monsoon onset (approximately three weeks earlier than observations), but captures the end of the monsoon quite well. This leads to a simulated monsoon that is approximately two weeks longer than that observed. We note, however, that there is significant variability

between ensemble members in their estimates of the NAM timings, with more variability in the NAM start time than in the end time.

Despite the earlier start time in the NAM using CORDEX, the simulations still produce pronounced monsoon seasonality, with which we may calculate changes through the end of the century. By the end of the century, the NAM is projected to start approximately one week later, end approximately three weeks later, and last approximately two weeks longer than the historical period (Table 2). We again note the sizeable spread in the NAM characteristics across simulations, but almost all models suggest a delay in the onset and a lengthening of the monsoon season. The projected delay in the NAM seen in the NA-CORDEX ensemble is similar to that seen in the larger CMIP5 ensemble (Cook and Seager 2013) as is the relatively small change in precipitation rates during the monsoon season (Seager and Vecchi 2010), though an increase in extreme monsoonal precipitation is expected. The changes in seasonality over the region, considering NAM in the context of other processes responsible for precipitation over the region, are discussed further in Section 5.

d. Case study: five major cities

Finally, we have conducted a case study of changes in precipitation over five major cities in Northern Mexico: Ciudad Juárez, Monterrey, Culiacán, Hermosillo, and Tijuana (Fig. 13). These cities were chosen because they are all major social and economic hubs and their locations are spread out throughout most of Northern Mexico. Therefore, cities shown in Fig. 13 represent a somewhat comprehensive selection of climate regimes in this region and help us best exemplify the variety in timing and intensity of precipitation changes in NA-CORDEX projections.

There are several notable differences in local precipitation changes over these cities compared to the larger regional changes. For example, although precipitation is projected to decrease for Summer and increase for Fall over most of Northern Mexico, drier Summers are only evident in Monterrey and Culiacán (Figs. 13b,c), while wetter Falls are only

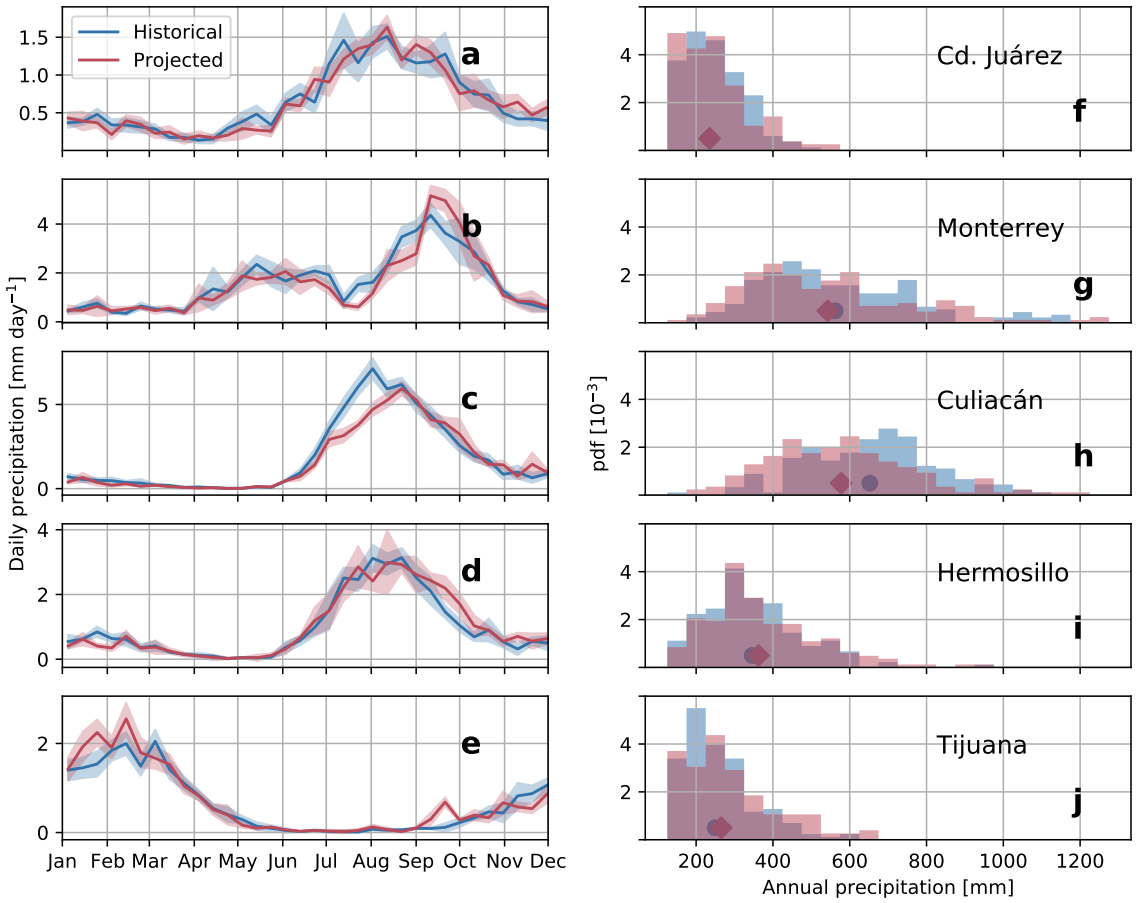

Figure 13. Changes in precipitation in major metropolitan areas. For each city, (a-e) show multimodel averages of daily precipitation throughout the year are shown with 90% confidence intervals in shading. (f-j) Histograms of accumulated yearly precipitation are shown in color, while circles and diamonds show mean historical and projected values respectively.

projected for Monterrey, Hermosillo, and Tijuana (Figs. 13b,d,e). Precipitation changes over Ciudad Juárez are small (Fig. 13a), while Tijuana is the only city where increased Winter precipitation may be expected from the NA-CORDEX projections (Fig. 13e).

Changes in the timing of local precipitation are crucial for urban populations and decision makers. Monterrey is projected to see a reduction in precipitation between late June and September (Fig. 13b), when heat stress and demand on water resources are greatest. Even

though the annual mean daily precipitation for Monterrey and its surroundings is projected to only change slightly (Figs. 4a, 13g), the wetter Falls that compensate for drier Summers can exacerbate risk of flooding that has historically affected the city (Aguilar-Barajas et al. 2019). In Culiacán, drier Summers are likely to impact the early growing season and thus shift agricultural activities that sustain the economy of Sinaloa.

Histograms of yearly cumulative precipitation provide more insight into possible challenges facing decision makers in northern Mexican cities (Figs. 13f-j). The frequency of years with lower cumulative precipitation is projected to increase for Ciudad Juárez, Monterrey, and Culiacán (Figs. 13f-h), while high-precipitation years are projected to increase in all cities except Culiacán, where the wettest years are still projected to be wetter than in historical simulations (Fig. 13h). These results are consistent with projected changes in extreme precipitation at the regional level (Fig. 6) and across all of Northern Mexico (Fig. 9), pointing to the disproportionate role of extreme events in future hydrological changes in the region.

5. Discussion and Conclusions

In this study, we have used the dynamically-downscaled NA-CORDEX ensemble to comprehensively examine future trends in both mean and extreme precipitation over Northern Mexico. We started by conducting a comparison of historical simulations from the NA-CORDEX ensemble with observations from MSWEP. The simulations show excellent agreement with observations, both in the annual-average and across the seasons (Figures 1-3). While the simulations in the NA-CORDEX ensemble under-precipitate, the spatial patterns of simulated mean and extreme precipitation are highly correlated with observations and the seasonality in mean and extreme precipitation is similarly consistent between simulations and observations. Given the strong agreement between historical simulations and observations, the NA-CORDEX ensemble is appropriate for studying future changes in precipitation over the region.

One aspect of Mexican hydroclimate that the models do not necessarily capture is the midsummer drought, which leads to a double-peak in the summertime precipitation over south and northeastern regions of Mexico (Perdigón-Morales et al. 2018; García-Franco et al. 2021). Figure 3a illustrates that the midsummer drought (i.e. the dip in mean precipitation around August) is not captured by NA-CORDEX or MSWEP, which is not altogether surprising as the magnitude of the decrease in precipitation is relatively small, since the only states that experience the midsummer drought in Northern Mexico are Tamaulipas and Nuevo León. Nevertheless, the ensemble's inability to capture the midsummer drought deserves follow-up study, particularly given the impacts of the drought on agriculture and industry (Englehart and Douglas 2000).

Simulations suggest that the spatial pattern of future trends in mean precipitation is strikingly similar to that of extreme precipitation (Figures 4, 6). Regions projected to experience a decrease in mean precipitation are likewise projected to experience a decrease in extreme precipitation, and vice-versa. The magnitudes of the projected changes are relatively small (approximately 10% for both mean and extreme precipitation) and well below the increase that would be expected from thermodynamics alone (Figures 10 and 11). However, the frequency of extreme precipitation events is likely to increase by 50-100%, suggesting that the water the region depends on for agriculture will be more intermittent and management practices will have to adapt accordingly (Figure 9).

Relatively small changes in annually-averaged precipitation mask a significant seasonal change in both mean and extreme precipitation. The largest changes are projected to occur during Spring and Fall, when precipitation is expected to decrease and increase, respectively, with lower magnitude and regionally-dependent changes during Winter and Summer. This shift in maximum precipitation to later in the year is consistent with a delayed onset of the North American Monsoon. While drying is projected to occur in certain regions throughout the year, drying during the summertime is particularly significant given that Northern Mexico already experiences little precipitation and significant heat stress during this time of the year (Hallack-Alegria and Watkins 2007). Chihuahua, Sinaloa and Sonora, which

amount for 72% of Northern Mexico's agricultural output (INEGI 2020), are all projected to experience strong drying during the Spring and Summer months, which would have major implications for Northern Mexico's food availability and security. Spring and Summer drying were likewise seen in the downscaled simulations of Cavazos and Arriaga-Ramírez (2012), who used an earlier generation of models to analyze changes in precipitation over the sub-region of Baja California, as well as Cook and Seager (2013) who likewise observed a shift of the monsoon to later in the year.

The projected large, widespread decreases in seasonal precipitation (Figure 4b-e) are likely to further stress on Northern Mexican water resources and public health infrastructure. For example, historical records have shown a positive association between Fall and Winter precipitation rates and the incidence of Dengue fever in the region (Brunkard et al. 2008). The increases in both mean and extreme precipitation seen here, as well as the projected warming, suggest that the environment may become conducive to the spread of Dengue through the end of the century (Chowell and Sanchez 2006).

Some of the changes in precipitation, particularly over the western states during late Spring and Summer, are likely due to changes in the North American Monsoon. Based on the NA-CORDEX ensemble, the NAM is projected to begin and end later, and hence last longer, thereby shifting and extending the period of heavy rainfall later in the year. This shift may exacerbate drought conditions over portions of the region, particularly given the high heat stress and demand for water resources during the Spring. While there is reasonable agreement between the simulations in the shift of the monsoon later in the year with results from earlier studies (Cook and Seager 2013), there are significant model differences in the timing of the end of the monsoon. Follow up studies to more precisely quantify the shift of the NAM using a larger ensemble may be advantageous.

The large projected decrease in Spring precipitation may also be due to changes in atmospheric rivers responsible for providing the region with precipitation during the Winter and Spring. Our results suggest that there may be a weakening or a change in timing of atmospheric rivers transporting moisture to northwest Mexico, although we are not able to

investigate the processes responsible for advection of moisture over the region due to the lack of NA-CORDEX data at different atmospheric levels.

Furthermore, an increase in the rain rate of future Atlantic tropical cyclones, particularly those that propagate over or near Northern Mexico, may be responsible for the increase in extreme precipitation during the Fall, as seen in Knutson et al. (2020). Given that the primary genesis regions in the Eastern North Pacific and Atlantic regions are outside of the NA-CORDEX domain (Tippett et al. 2011), the NA-CORDEX ensemble has non-negligible bias in its projections of mean and extreme precipitation, and this bias is particularly large for the western coast of Mexico (Rendfrey et al. 2021). Despite this bias, the projected increase in tropical cyclone-driven precipitation over the region is consistent with Dominguez et al. (2021). Based on our results, we hypothesize that the extension of the NAM, which primarily impacts the western portion of the region, coupled with the increase in tropical-cyclone precipitation from Atlantic tropical cyclones over the eastern portion of the region may be responsible for the projected increase in mean and extreme precipitation across the region during Fall.

While we have conducted a comprehensive study of the future trends in mean and extreme precipitation over Northern Mexico through the end of the century, we have not been able to identify the dynamical drivers responsible for these trends. A follow-up study analyzing the change in circulation patterns over the region is essential to provide a full understanding of the physical processes driving this change. Based on the results presented here, we expect that there is a significant slowdown of the dynamics driving changes in precipitation (particularly extreme precipitation) over this region. Nevertheless, the analysis presented here is an important and necessary first step in quantifying changes in the hydroclimate of Northern Mexico, which is required for stakeholders and local agencies to prepare for the increased intermittency and significant seasonal changes in precipitation over this important yet understudied region.

Acknowledgments. The authors thank Dr. Jorge García-Franco for providing helpful feedback on an earlier version of this manuscript. R. Nazarian, B. Matijevic, J. Vizzard, and C. Agostino gratefully acknowledge support from Fairfield University, including the College of Arts and Sciences, Science Institute, and Provost's Office. R. Nazarian, B. Matijevic, J. Vizzard, and C. Agostino also gratefully acknowledge support from the NASA Connecticut Space Grant Consortium, award P-1704. N. Brizuela was supported by Consejo Nacional de Ciencia y Tecnología and UC Mexus. N. Lutsko was supported by NSF grant OCE-2023483. More information about conducting undergraduate research with CORDEX can be found in Nazarian (2021).

Data availability statement. All NA-CORDEX simulations used in this study are freely available on the NCAR Climate Data Gateway: `https://www.earthsystemgrid.org/search/cordexsearch.html`. All MSWEP data are freely available on the GloH2O portal: `https://www.gloh2o.org/mswep/`.

References

Abbott, T., T. Cronin, and T. Beucler, 2020: Convective dynamics and the response of precipitation extremes to warming in radiative–convective equilibrium. *Journal of the Atmospheric Sciences*, **77**, 1637–1660.

Adams, D., and A. Comrie, 1997: The north american monsoon. *Bulletin of the American Meteorological Society*, **78 (10)**, 2197–2214, https://doi.org/https://journals.ametsoc.org/view/journals/bams/78/10/1520-0477_1997_078_2197_tnam_2_0_co_2.xml.

Aguilar-Barajas, I., N. P. Sisto, A. I. Ramirez, and V. Magaña-Rueda, 2019: Building urban resilience and knowledge co-production in the face of weather hazards: flash floods in the monterrey metropolitan area (mexico). *Environmental Science & Policy*, **99**, 37–47, https://doi.org/https://doi.org/10.1016/j.envsci.2019.05.021, URL https://www.sciencedirect.com/science/article/pii/S1462901118309146.

573 Almazroui, M., and Coauthors, 2021: Projected changes in temperature and precip-
574 itation over the united states, central america, and the caribbean in cmip6 gcms.
575 *Earth Systems and Environment*, **5 (1)**, 1–24, https://doi.org/https://doi.org/10.1007/
576 s41748-021-00199-5.

577 Andrews, T., J. Gregory, M. Webb, and K. Taylor, 2012: Forcing, feedbacks and climate
578 sensitivity in cmip5 couples atmosphere-ocean climate models. *Geophysical Research*
579 *Letters*, **39**, L09 712.

580 Ashfaq, M., D. Rastogi, R. Mei, S.-C. Kao, S. Gangrade, B. S. Naz, and D. Touma, 2016:
581 High-resolution ensemble projections of near-term regional climate over the continental
582 united states. *Journal of Geophysical Research: Atmospheres*, **121 (17)**, 9943–9963,
583 https://doi.org/https://doi.org/10.1002/2016JD025285.

584 Ban, N., J. Schmidli, and C. Schär, 2015: Heavy precipitation in a changing climate: Does
585 short-term summer precipitation increase faster? *Geophysical Research Letters*, **42 (4)**,
586 1165–1172, https://doi.org/https://doi.org/10.1002/2014GL062588.

587 Barlow, M., S. Nigam, and E. Berbery, 1998: Evolution of the north american monsoon
588 system. *Journal of Climate*, **11 (9)**, 2238–2257, https://doi.org/https://doi.org/10.1175/
589 1520-0442(1998)011⟨2238:EOTNAM⟩2.0.CO;2.

590 Beck, H. E., E. F. Wood, M. Pan, C. K. Fisher, D. M. Miralles, A. I. J. M. van Dijk, T. R.
591 McVicar, and R. F. Adler, 2019: Mswep v2 global 3-hourly 0.1◦ precip- itation: method-
592 ology and quantitative assessment. *Bulletin of the American Meteorological Society*, **100**,
593 473–500.

594 Beck, H. E., and Coauthors, 2017: Global-scale evaluation of 22 precipitation datasets using
595 gauge observations and hydrological modeling. *Hydrology and Earth System Sciences*,
596 **21**, 6201–6217.

597 Boos, W., and S. Pascale, 2021: Mechanical forcing of the north american monsoon by
598 orography. *Nature*, **599**, 611–615.

599 Breña Naranjo, J., A. Pedrozo-Acuña, O. Pozos-Estrada, S. Jiménez-López, and M. López-
600 López, 2015: The contribution of tropical cyclones to rainfall in mexico. *Physics and*
601 *Chemistry of the Earth, Parts A/B/C*, **83-84**, 111–122.

602 Brunkard, J. M., E. Cifuentes, and S. J. Rothenberg, 2008: Assessing the roles of tempera-
603 ture, precipitation, and enso in dengue re-emergence on the texas-mexico border region.
604 *Salud pública de México*, **50 (3)**, 227–234.

605 Bukovsky, M., and L. Mearns, 2020: Regional climate change projections from na-cordex
606 and their relation to climate sensitivity. *Climatic Change*, **162**, 645–665.

607 Cannon, A., 2018: Multivariate quantile mapping bias correction: an n-dimensional
608 probability density function transform for climate model simulations of multiple
609 variables. *Climate Dynamics*, **50 (1)**, 31–49, https://doi.org/https://doi.org/10.1007/
610 s00382-017-3580-6.

611 Caparas, M., Z. Zobel, A. D. Castanho, and C. R. Schwalm, 2021: Increasing risks of
612 crop failure and water scarcity in global breadbaskets by 2030. *Environmental Research*
613 *Letters*, **16 (10)**, 104 013, https://doi.org/https://doi.org/10.1088/1748-9326/ac22c1.

614 Cavazos, T., and S. Arriaga-Ramírez, 2012: Greenhouse warming and the 21st century
615 hydroclimate of southwestern north america. *Journal of Climate*, **25**, 5904–5915.

616 Chowell, G., and F. Sanchez, 2006: Climate-based descriptive models of dengue fever: The
617 2002 epidemic in colima, mexico. *Journal of Environmental Health*, **69**, 40–44.

618 Colorado-Ruiz, G., T. Cavazos, J. Salinas, P. DeGrau, and R. Ayala, 2018: Climate change
619 projections from coupled model intercomparison project phase 5 multi-model weighted
620 ensembles for mexico, the north american monsoon, and the mid-summer drought region.
621 *International Journal of Climatology*, **38**, 5699–5716.

Cook, B., and R. Seager, 2013: The response of the north american monsoon to increased greenhouse gas forcing. *Journal of Geophysical Research: Atmospheres*, **118**, 1690–1699.

Dettinger, M. D., F. M. Ralph, T. Das, P. J. Neiman, and D. R. Cayan, 2011: Atmospheric rivers, floods and the water resources of california. *Water*, **3 (2)**, 445–478, https://doi.org/https://doi.org/10.3390/w3020445, URL https://www.mdpi.com/2073-4441/3/2/445.

Di Luca, A., R. de Elia, and R. Laprise, 2012: Potential for added value in precipitation simulated by high-resolution nested regional climate models and observations. *Climate Dynamics*, **38**, 1229–1247.

Díaz Caravantes, R. E., A. L. Castro Luque, and P. Aranda Gallegos, 2014: Mortalidad por calor natural excesivo en el noroeste de méxico: Condicionantes sociales asociados a esta causa de muerte. *Frontera norte*, **26 (52)**, 155–177.

Diffenbaugh, N., J. Pal, R. Trapp, and F. Giorgi, 2005: Fine-scale processes regulate the response of extreme events to global climate change. *Proceedings of the National Academy of Sciences*, **102**, 15 774–15 778.

Dominguez, C., J. Done, and C. Bruyere, 2021: Future changes in tropical cyclone and easterly wave characteristics over tropical north america. *Oceans*, **2**, 429–447.

Donat, M., A. Lowry, L. Alexander, P. O'Gorman, and N. Maher, 2016: More extreme precipitation in the world's dry and wet regions. *Nature Climate Change*, **6**, 508–513.

Englehart, P., and A. Douglas, 2000: Dissecting the macro-scale variations in mexican maize yields (1961-1997). *Geographical and Environmental Modeling*, **1**, 65–81.

Flato, G., J. Marotzke, B. Abiodun, P. Braconnot, S. Chou, W. Collins, and J. Zhang, 2014: Evaluation of climate models. *Climate change 2013 - the physical science basis: working group I constribution to the fifth assessment report of the intergovernmental panel on climate change*, Cambridge University Press, 741–866.

García-Franco, J., S. Osprey, and L. Gray, 2021: A wavelet transform method to determine monsoon onset and retreat from precipitation time-series. *International Journal of Climatology*, **41**, 5295–5317.

Geil, K., and X. Serra, Y.L. Zeng, 2013: Assessment of cmip5 model simulations of the north american monsoon system. *Journal of Climate*, **26**, 8787–8801.

Hallack-Alegria, M., and D. Watkins, 2007: Annual and warm season drought intensity–duration–frequency analysis for sonora, mexico. *Journal of Climate*, **20**, 1897–1909.

He, C., T. Li, and W. Zhou, 2020: Drier north american monsoon in contrast to asian–african monsoon under global warming. *Journal of Climate*, **33 (22)**, 9801–9816, https://doi.org/ https://doi.org/10.1175/JCLI-D-20-0189.1.

INEGI, 2020: Encuesta nacional agropecuaria 2019.

Jáuregui, E., 2003: Climatology of landfalling hurricanes and tropical storms in mexico. *Atmósfera*, **16 (4)**, 193–204.

Kirchmeier-Young, M., F. Zwiers, N. Gillett, and A. Cannon, 2017: Attributing extreme fire risk in western canada to human emissions. *Climatic Change*, **144 (2)**, 365–379, https://doi.org/https://doi.org/10.1007/s10584-017-2030-0.

Knutson, T., and Coauthors, 2020: Tropical cyclones and climate change assessment: Part ii: Projected response to anthropogenic warming. *Bulletin of the American Meteorological Society*, **101**, 100 382.

Leung, L., L. Mearns, F. Giorgi, and R. Wilby, 2003: Regional climate research: needs and opportunities. *Bulletin of the American Meteorological Society*, **84**, 89–95.

Li, L., Y. Wang, L. Wang, Q. Hu, Z. Zhu, L. Li, and C. Li, 2022: Spatio-temporal accuracy evaluation of mswep daily precipitation over the huaihe river basin, china: A comparison study with representative satellite- and reanalysis-based products. *Journal of Geographical Sciences*, **32**, 2271–2290.

672 Lopez-Cantu, T., A. Prein, and C. Samaras, 2020: Uncertainties in future u.s. extreme
673 precipitation from downscaled climate projections. *Geophysical Research Letters*, **47 (7)**,
674 e2019GL086 797, https://doi.org/https://doi.org/10.1029/2019GL086797.

675 Lucas-Picher, P., R. Laprise, and K. Winger, 2017: Evidence of added value in north
676 american regional climate model hindcast simulations using ever-increasing horizontal
677 resolutions. *Climate Dynamics*, **48 (7)**, 2611—-2633, https://doi.org/https://doi.org/10.
678 1007/s00382-016-3227-z.

679 Lutsko, N., and T. Cronin, 2018: Increase in precipitation efficiency with surface warming
680 in radiative-convective equilibrium. *Journal of Advances in Modeling Earth Systems*, **10**,
681 2992–3010.

682 Magaña, V., E. Herrera, C. Ábrego Góngora, and J. Ávalos, 2021: Socioeconomic drought
683 in a mexican semi-arid city: Monterrey metropolitan area, a case study. *Frontiers in*
684 *Water*, **3**, 579 564.

685 Martinez-Villalobos, C., and J. Neelin, 2019: Why do precipitation intensities tend to follow
686 gamma distributions? *Journal of the Atmospheric Sciences*, **76**, 3611–3631.

687 McGinnis, S., and L. Mearns, 2021: Building a climate service for north america based on
688 the na-cordex data archive. *Climate Services*, **22 (2405-8807)**, 100 233, https://doi.org/
689 https://doi.org/10.1016/j.cliser.2021.100233.

690 Mo, K. C., 2000: Intraseasonal modulation of summer precipitation over north america.
691 *Monthly Weather Review*, **128 (5)**, 1490–1505, https://doi.org/https://doi.org/10.1175/
692 1520-0493(2000)128⟨1490:IMOSPO⟩2.0.CO;2.

693 Muller, C., and Y. Takayabu, 2020: Response of precipitation extremes to warming: what
694 have we learned from theory and idealized cloud-resolving simulations, and what remains
695 to be learned? *Environmental Research Letters*, **15**, 035 001.

Myhre, G., and Coauthors, 2019: Frequency of extreme precipitation increases extensively with event rareness under global warming. *Scientific Reports*, **9**.

Nazarian, R., 2021: The use of model intercomparison projects in engaging undergraduates in climate change research. *Scholarship and Practice of Undergraduate Research*, **5**, 27–28.

Nazarian, R., J. Vizzard, C. Agostino, and N. Lutsko, 2022: Projected changes in future extreme precipitation over the northeast us in the na-cordex ensemble. *Journal of Applied Meteorology and Climatology*, **61**, 1649–1668.

Ortega-Gaucin, D., and I. Velasco, 2013: Aspectos socioeconómicos y ambientales de las sequías en méxico. *Aqua-lac*, **5 (2)**, 78–90.

O'Gorman, P., 2015: Precipitation extremes under climate change. *Current climate change reports*, **1 (2)**, 49–59, https://doi.org/https://doi.org/10.1007/s40641-015-0009-3.

Pascale, S., W. Boos, S. Bordoni, T. Delworth, S. Kapnick, H. Murakami, G. Vecchi, and W. Zhang, 2017: Weakening of the north american monsoon with global warming. *Nature Climate Change*, **7**, 806–812.

Pendergrass, A., F. Lehner, B. Sanderson, and Y. Xu, 2015: Does extreme precipitation intensity depend on the emission scenario? *Geophysical Research Letters*, **42**, 8767–8774.

Perdigón-Morales, J., R. Romero-Centeno, P. Pérez, and B. Barrett, 2018: The midsummer drought in mexico: Perspectives on duration and intensity from the chirps precipitation database. *International Journal of Climatology*, **38**, 2174–2186.

Rajczak, J., P. Pall, and C. Schar, 2013: Projections of extreme precipitation events in regional climate simulations for europe and the alpine region. *Journal of Geophysical Research: Atmospheres*, **118**, 3610–3626.

Rendfrey, T., M. Bukovsky, R. McCrary, and R. Fuentes-Franco, 2021: An assessment of tropical cyclones in north american cordex wrf simulations. *Weather and Climate Extremes*, **34**, 100 382, https://doi.org/https://doi.org/10.1016/j.wace.2021.100382.

Reyes, S., M. Douglas, and R. Maddox, 1994: El monzón del suroeste de norteamérica (travason/swamp). *Atmósfera*, **7 (2)**, 117–137, https://doi.org/https://www.redalyc.org/pdf/565/56507204.pdf.

Rutz, J., and W. J. Steenburgh, 2012: Quantifying the role of atmospheric rivers in the interior western united states. *Atmospheric Science Letters*, **13 (4)**, 257–261, https://doi.org/https://doi.org/10.1002/asl.392.

Schär, C., and Coauthors, 2016: Percentile indices for assessing changes in heavy precipitation events. *Climatic Change*, **137 (1)**, 201–216, https://doi.org/https://doi.org/10.1007/s10584-016-1669-2.

Seager, R., and G. Vecchi, 2010: Greenhouse warming and the 21st century hydroclimate of southwestern north america. *Proceedings of the National Academy of Sciences*, **107**, 21 277–21 282.

Sharifi, E., J. Eitzinger, and W. Dorigo, 2019: Performance of the state-of-the-art gridded precipitation products over mountainous terrain: a regional study over austria. *Remote Sensing*, **11**.

Tabari, A., 2020: Climate change impact on flood and extreme precipitation increases with water availability. *Scientific Reports*, **10**, 13 768.

Tippett, M., S. Camagro, and A. Sobel, 2011: A poisson regression index for tropical cyclone genesis and the role of large-scale vorticity in genesis. *Journal of Climate*, **24**, 2335–2357.

Xu, Z., Z. Wu, H. He, X. Wu, J. Zhou, Y. Zhang, and X. Guo, 2019: Evaluating the accuracy of mswep v2.1 and its performance for drought monitoring over mainland china. *Atmospheric Research*, **226**, 17–31.

Zhang, Y., T. Li, B. Wang, and G. Wu, 2002: Onset of the summer monsoon over the indochina peninsula: Climatology and interannual variations. *Journal of Climate*, **15 (22)**, 3206–3221, https://doi.org/https://doi.org/10.1175/1520-0442.